CONTRIBUTIONS TO JOINED-WING AEROELASTICITY

Luciano Demasi[1] **and Eli Livne**[2]

[1]Assistant Professor
Department of Aerospace Engineering & Engineering Mechanics, San Diego State University,
San Diego, CA, 92182-1308, USA
ldemasi@mail.sdsu.edu

[2]Professor
Department of Aeronautics and Astronautics, University of Washington,
Seattle, WA, 98195-2400, USA
eli@aa.washington.edu

Keywords. Joined-wings, nonlinear aeroelasticity, flutter, unsteady aerodynamics, reduced order models

Abstract. In previous works the authors introduced a procedure for coupling linear modally reduced frequency-domain unsteady aerodynamic codes such as the Doublet Lattice and other panel methods with full order geometrically nonlinear finite element structural models for the analysis of high aspect ratio wings, Joined Wings, and other configurations with important geometric structural nonlinearities. A procedure to couple the full order (rather than modal based) linear unsteady aerodynamics and full order geometrically nonlinear structures was also presented.
Using the procedure previously introduced, in this paper the aeroelastic behavior of 2 test Joined Wing configurations is analyzed in detail and the effects of the position of the joint are discussed. It is shown that the present methodology is a useful tool for the study of new complex geometrically nonlinear non-planar configurations when the steady/unsteady aerodynamic forces involved are linear.

1 INTRODUCTION

Aerodynamic and structural nonlinearities can play an important role in aeroelasticity. This paper focuses on the case in which the source of nonlinearity is structural geometric, allowing large displacements and rotations. In the past nonlinear high aspect-ratio configurations were analyzed using beam models. Geometrically nonlinear beam models were also adopted in the modeling of high-altitude long-endurance UAVs. Such high aspect ratio wings deform considerably under load and can display large deformations. But even relatively small deformations can lead to significant geometrical nonlinear effects. Such are the cases of the strut-braced wing and the Joined-Wing (JW) configurations [1]. Geometric structural nonlinearity has been shown to be extremely important for the aeroelastic simulation of low aspect ratio plate-like wings. Theoretical and experimental studies of plate-like and beam-like wings with geometric structural nonlinearity have indeed confirmed the importance of understanding where structural geometric nonlinear effects become aeroelastically important and of accounting for them. An adequate modeling of the nonlinearity in the structural area for general configurations requires the use of the nonlinear Finite Element Method. But when nonlinear finite elements are used to model a geometrically nonlinear structure they are usually coupled with computational fluid dynamics (CFD) models for the flow, as it is natural to seek detailed modeling

capable of capturing all nonlinearities in all disciplines contributing to aeroelastic interactions [2,3]. But unsteady CFD simulations are computationally demanding and require a lengthy model set-up and meshing processes. In the case of high aspect-ratio configurations and structural geometric nonlinearity 2D linear potential unsteady aerodynamic models in the time domain have been used with considerable success to capture aeroelastic behavior in subsonic flow. Such models can be used to also model dynamic stall effects. For low aspect ratio wings, where deformation is small enough that the unsteady aerodynamic loads are linear but large enough to cause structural geometric nonlinearity, dedicated time marching vortex lattice models proved adequate. These dedicated time-marching vortex lattice models have been limited so far to planar configurations of simple planforms and to incompressible flow. For the 3-dimensional (3D) case, unsteady aerodynamic linear potential codes such as the Doublet Lattice Methods (DLM), PANAIR [4], or ZAERO [5–7] have been the backbone of aeroelastic analysis and certification since the 1970s with great success. As long as small angles of attack are involved with no major shock waves or separation, such methods are accurate, useful, and thoroughly validated.

They are based on a frequency domain formulation, where unsteady aerodynamic force terms are calculated for simple harmonic motion at given reduced frequencies. These need to be transformed to the time domain for integration with time domain nonlinear structural models. The classical panel-based unsteady aerodynamic procedures are also based on a modal approach, in which the modeling of structural behavior is reduced in order by using generalized coordinates in the form of various mode shape bases.
Linear compressible unsteady aerodynamic theory has already been successfully used for the aeroelastic modeling of structurally nonlinear wing configurations [8, 9]. In these previous efforts the unsteady aerodynamic models were modally reduced, and a special procedure based on the Least Square Method was introduced to transform the modally reduced order aerodynamic matrices to the full order FE matrices. The methodology proved to be effective for planar configurations and non-planar configurations when structural behavior is geometrically nonlinear, but overall deformation of the lifting surfaces involved is smooth and global in nature - the kind of overall deformation well captured by a well selected modal base. If, however, overall deformation of the configuration displays local effects not well captured by the set of deformation mode shapes used, a modal approach will lead to inaccuracy of the unsteady aerodynamic models.

An alternative approach is possible [10]. A full order (not modally reduced) aerodynamic model) corresponding to the full aerodynamic panel mesh involved, is coupled with a full order nonlinear structural model. The method can be used in all the cases in which the aerodynamic modal based model [8,9] is less accurate (highly geometrically nonlinear Joined Wings), but in which the aerodynamics can still be considered linear and the flow attached. Such an aerodynamically full order capability allows studies of the accuracy and performance of modally reduced aerodynamic models.

2 DISPLACEMENT VECTORS, CUMULATIVE DISPLACEMENT VECTORS, LINEAR UNSTEADY AERODYNAMICS, AND NONLINEAR STRUCTURAL MODEL

The Displacement and Cumulative Displacement Vectors are key quantities used in the derivations presented in this paper. The displacement vector $\boldsymbol{u}$ is relative to the configu-

ration at the beginning of the current iteration (within a time step for the dynamic case and within a load step for the static case) in a Newton Raphson procedure. The vector which contains the coordinates of all the structural nodes of the wing system is $\boldsymbol{x}$. The coordinates define the configuration before the displacement vector is added.

An Updated Lagrangian Formulation [11–13] is used here and so the coordinates of the nodes are continuously updated during the iteration process.
The quantity $\boldsymbol{x}^{\alpha=0}$ represents the coordinate vector of all structural nodes at a reference aerodynamic configuration with zero angle of attack. Aerodynamic panels are defined based on the geometry of that reference configurations and structural motion away from the reference configuration is assumed small. This simplifies aerodynamic modeling in this work, since aerodynamic influence coefficients can be determined once with respect to the reference aerodynamic configuration.
The cumulative displacement vector is designated $\boldsymbol{U}$ and is defined as the summation of all the displacements that have occurred during the iteration process up to the current iteration. Basically, the coordinates at a particular load level are obtained by adding the vector of the coordinates in the undeformed configuration ($\boldsymbol{x}^{\alpha=0}$) to the translational part of all the displacements that the structure was subjected to all the previous load levels.
The Doublet Lattice Method is used here as a representative linear unsteady aerodynamic method.
The geometrically nonlinear structural model for thin-plate aerospace structures used here is created using flat triangular elements [11–13]. A tangent stiffness matrix is built for given structural shape and internal stress distributions by combining linear elastic and geometric stiffness matrices. The geometric stiffness matrix is derived by applying a load perturbation method, when the gradient (with respect to the coordinates) of the nodal force vector (when the stresses are considered fixed) is calculated. Rigid body motion is removed based on [11] and unbalanced loads are calculated as the nonlinear analysis (Newton Raphson) progresses.

3 AEROELASTIC TIME DOMAIN SIMULATIONS WITH FULL ORDER NONLINEAR STRUCTURE AND FULL ORDER LINEAR UNSTEADY AERODYNAMICS

The boundary condition associated with the unsteady aerodynamics can be written in the frequency domain as follows:

$$\boldsymbol{w}\left(j\omega\right) = j\frac{\omega}{V_\infty}\boldsymbol{\mathcal{Z}}_{\mathrm{loc}}\left(j\omega\right) + \frac{\mathrm{d}\boldsymbol{\mathcal{Z}}_{\mathrm{loc}}\left(j\omega\right)}{\mathrm{d}x} \tag{1}$$

$\boldsymbol{w}\left(j\omega\right)$ is a vector containing the normalized normalwash calculated at the control points of the aerodynamic panels, j is the complex unit, ω is the circular frequency and the vector $\boldsymbol{\mathcal{Z}}_{\mathrm{loc}}\left(j\omega\right)$ contains the local out-of-plane motion at the control point locations.
Using the infinite plate spline method the spline matrices $\boldsymbol{A}_3$ and $\boldsymbol{A}_3^\star$ can be obtained. It is possible to relate (see References [8, 9]) the out-of-plane motion and slopes with the cumulative displacement vector $\boldsymbol{U}\left(j\omega\right)$ as follows:

$$\frac{\mathrm{d}\boldsymbol{\mathcal{Z}}_{\mathrm{loc}}\left(j\omega\right)}{\mathrm{d}x} = \boldsymbol{A}_3 \cdot \boldsymbol{U}\left(j\omega\right) \tag{2}$$

$$\boldsymbol{\mathcal{Z}}_{\mathrm{loc}}\left(j\omega\right) = \boldsymbol{A}_3^\star \cdot \boldsymbol{U}\left(j\omega\right) \tag{3}$$

Substituting equations 2 and 3 into the relation which gives the normalwash (equation 1) we get:

$$\boldsymbol{w}\left(j\omega\right)=\left[j\frac{\omega}{V_{\infty}}\boldsymbol{A}_{3}^{\star}+\boldsymbol{A}_{3}\right]\cdot\boldsymbol{U}\left(j\omega\right) \tag{4}$$

The fundamental doublet lattice equation relates the dimensionless normalwash with the dimensionless pressure jump as follows:

$$\boldsymbol{w}\left(j\omega\right)=\boldsymbol{A}^{D}\left(j\omega\right)\cdot\Delta\boldsymbol{p}\left(j\omega\right) \tag{5}$$

$\boldsymbol{A}^{D}\left(j\omega\right)$ is named as *normalwash factor matrix*. Inverting equation 5 and using equation 4 it is possible to express the dimensionless pressure vector as a function of the cumulative displacement vector:

$$\Delta\boldsymbol{p}\left(j\omega\right)=\left[\boldsymbol{A}^{D}\left(j\omega\right)\right]^{-1}\boldsymbol{w}\left(j\omega\right)=\left[\boldsymbol{A}^{D}\left(j\omega\right)\right]^{-1}\cdot\left[j\frac{\omega}{V_{\infty}}\boldsymbol{A}_{3}^{\star}+\boldsymbol{A}_{3}\right]\cdot\boldsymbol{U}\left(j\omega\right) \tag{6}$$

For a generic panel the aerodynamic force, applied at the load point of that panel is obtained by multiplying the dynamic pressure by some geometrical quantities of the panel and by the dimensionless pressure jump. If this fact is extended to all the wing system, it can be deduced that the vector which contains the scalar components of the aerodynamic forces of all the panels is written as a product between the fraction of the dynamic pressure and a matrix $\boldsymbol{I}_{D}$ which depends on the geometry. This matrix has to multiply the vector containing all the pressure jumps. Thus

$$\boldsymbol{L}\left(j\omega\right)=\frac{1}{2}\rho_{\infty}V_{\infty}^{2}\boldsymbol{I}_{D}\cdot\Delta\boldsymbol{p}\left(j\omega\right) \tag{7}$$

$\boldsymbol{L}\left(j\omega\right)$ has dimension $3N\times1$, $\boldsymbol{I}_{D}$ has dimension $3N\times N$, $\Delta\boldsymbol{p}\left(j\omega\right)$ has dimension $N\times1$. N is the number of aerodynamic boxes. The relation between the aerodynamic forces and the cumulative displacement vector can be found by substituting equation 6 into equation 7 as follows:

$$\boldsymbol{L}\left(j\omega\right)=\frac{1}{2}\rho_{\infty}V_{\infty}^{2}\boldsymbol{I}_{D}\cdot\left[\boldsymbol{A}^{D}\left(j\omega\right)\right]^{-1}\cdot\left[j\frac{\omega}{V_{\infty}}\boldsymbol{A}_{3}^{\star}+\boldsymbol{A}_{3}\right]\cdot\boldsymbol{U}\left(j\omega\right) \tag{8}$$

To elaborate equation 8 the introduction of the definitions of the matrices $\boldsymbol{\mathcal{B}}\left(j\omega\right)$ and $\boldsymbol{\mathcal{B}}^{\star}\left(j\omega\right)$ is required:

$$\boldsymbol{\mathcal{B}}\left(j\omega\right)=\left[\boldsymbol{A}^{D}\left(j\omega\right)\right]^{-1} \tag{9}$$

$$\boldsymbol{\mathcal{B}}^{\star}\left(j\omega\right)=j\frac{\omega}{V_{\infty}}\boldsymbol{\mathcal{B}}\left(j\omega\right)=j\frac{\omega}{V_{\infty}}\left[\boldsymbol{A}^{D}\left(j\omega\right)\right]^{-1} \tag{10}$$

With the help of equations 9 and 10 the aerodynamic loads (equation 8) in the frequency domain are written as

$$\boldsymbol{L}\left(j\omega\right)=\frac{1}{2}\rho_{\infty}V_{\infty}^{2}\boldsymbol{I}_{D}\cdot\left[\boldsymbol{\mathcal{B}}^{\star}\left(j\omega\right)\cdot\boldsymbol{A}_{3}^{\star}+\boldsymbol{\mathcal{B}}\left(j\omega\right)\cdot\boldsymbol{A}_{3}\right]\cdot\boldsymbol{U}\left(j\omega\right) \tag{11}$$

A Roger procedure is used to obtain a rational function approximation. Both matrices $\boldsymbol{\mathcal{B}}\left(j\omega\right)$ and $\boldsymbol{\mathcal{B}}^{\star}\left(j\omega\right)$ are considered and the same lag terms are used. This simplifies considerably the theory. The Roger procedure gives the following result:

$$\begin{cases}\boldsymbol{\mathcal{B}}\left(j\omega\right)=\boldsymbol{\mathcal{B}}_{0}+\left(j\omega\right)\frac{b}{V_{\infty}}\boldsymbol{\mathcal{B}}_{1}+\left(j\omega\right)^{2}\frac{b^{2}}{V_{\infty}^{2}}\boldsymbol{\mathcal{B}}_{2}+\sum_{i=1}^{\mathrm{N_{lag}}}\frac{j\omega}{j\omega+\frac{V_{\infty}}{b}\beta_{i}}\boldsymbol{\mathcal{B}}_{2+i}\\ \boldsymbol{\mathcal{B}}^{\star}\left(j\omega\right)=\boldsymbol{\mathcal{B}}_{0}^{\star}+\left(j\omega\right)\frac{b}{V_{\infty}}\boldsymbol{\mathcal{B}}_{1}^{\star}+\left(j\omega\right)^{2}\frac{b^{2}}{V_{\infty}^{2}}\boldsymbol{\mathcal{B}}_{2}^{\star}+\sum_{i=1}^{\mathrm{N_{lag}}}\frac{j\omega}{j\omega+\frac{V_{\infty}}{b}\beta_{i}}\boldsymbol{\mathcal{B}}_{2+i}^{\star}\end{cases} \tag{12}$$

Defining $\overline{\beta}_i = \frac{V_\infty}{b}\beta_i$, simplifying and using analytical continuation to expand from the imaginary axis to the Laplace domain adjacent to it $j\omega \to s$, it is possible to write the aerodynamic matrices in the Laplace domain, where s is the Laplace variable:

$$\begin{cases} \boldsymbol{\mathcal{B}}(s) = \boldsymbol{\mathcal{B}}_0 + s\dfrac{b}{V_\infty}\boldsymbol{\mathcal{B}}_1 + s^2\dfrac{b^2}{V_\infty^2}\boldsymbol{\mathcal{B}}_2 + \displaystyle\sum_{i=1}^{\mathrm{N_{lag}}} \frac{s}{s+\overline{\beta}_i}\boldsymbol{\mathcal{B}}_{2+i} \\ \boldsymbol{\mathcal{B}}^\star(s) = \boldsymbol{\mathcal{B}}_0^\star + s\dfrac{b}{V_\infty}\boldsymbol{\mathcal{B}}_1^\star + s^2\dfrac{b^2}{V_\infty^2}\boldsymbol{\mathcal{B}}_2^\star + \displaystyle\sum_{i=1}^{\mathrm{N_{lag}}} \frac{s}{s+\overline{\beta}_i}\boldsymbol{\mathcal{B}}_{2+i}^\star \end{cases} \tag{13}$$

Note that $\boldsymbol{\mathcal{B}}_0^\star = \mathbf{0}$. The reason for this is that $\boldsymbol{\mathcal{B}}_0^\star$ represents the *steady* counterpart of matrix $\boldsymbol{\mathcal{B}}^\star$ which is with only zeros in the steady case (see in particular its definition in equation 10). In the following derivation matrix $\boldsymbol{\mathcal{B}}_0^\star$ is kept to have the expressions of the Roger approximations for matrices $\boldsymbol{\mathcal{B}}^\star$ and $\boldsymbol{\mathcal{B}}$ formally identical (see equation 13). From equation 11 it is deduced that the aerodynamic forces in the Laplace domain can be written as

$$\boldsymbol{L}(s) = \frac{1}{2}\rho_\infty V_\infty^2 \boldsymbol{I}_D \cdot \left[\boldsymbol{\mathcal{B}}^\star(s)\cdot\boldsymbol{A}_3^\star + \boldsymbol{\mathcal{B}}(s)\cdot\boldsymbol{A}_3\right]\cdot\boldsymbol{U}(s) \tag{14}$$

Using equation 13 the aerodynamic loads (equation 14) are:

$$\boldsymbol{L}(s) = \left[\overline{\boldsymbol{\mathcal{A}}}_0 + s\overline{\boldsymbol{\mathcal{A}}}_1 + s^2\overline{\boldsymbol{\mathcal{A}}}_2 + \sum_{i=1}^{\mathrm{N_{lag}}} \frac{s}{s+\overline{\beta}_i}\overline{\boldsymbol{\mathcal{A}}}_{2+i}\right]\cdot\boldsymbol{U}(s) \tag{15}$$

were the following definitions have been introduced:

$$\begin{aligned} \overline{\boldsymbol{\mathcal{A}}}_0 &= \frac{1}{2}\rho_\infty V_\infty^2 \boldsymbol{I}_D\cdot\boldsymbol{\mathcal{B}}_0^\star\cdot\boldsymbol{A}_3^\star + \frac{1}{2}\rho_\infty V_\infty^2 \boldsymbol{I}_D\cdot\boldsymbol{\mathcal{B}}_0\cdot\boldsymbol{A}_3 \\ \overline{\boldsymbol{\mathcal{A}}}_1 &= \frac{1}{2}\rho_\infty V_\infty b \boldsymbol{I}_D\cdot\boldsymbol{\mathcal{B}}_1^\star\cdot\boldsymbol{A}_3^\star + \frac{1}{2}\rho_\infty V_\infty b \boldsymbol{I}_D\cdot\boldsymbol{\mathcal{B}}_1\cdot\boldsymbol{A}_3 \\ \overline{\boldsymbol{\mathcal{A}}}_2 &= \frac{1}{2}\rho_\infty b^2 \boldsymbol{I}_D\cdot\boldsymbol{\mathcal{B}}_2^\star\cdot\boldsymbol{A}_3^\star + \frac{1}{2}\rho_\infty b^2 \boldsymbol{I}_D\cdot\boldsymbol{\mathcal{B}}_2\cdot\boldsymbol{A}_3 \\ \overline{\boldsymbol{\mathcal{A}}}_{2+i} &= \frac{1}{2}\rho_\infty V_\infty^2 \boldsymbol{I}_D\cdot\boldsymbol{\mathcal{B}}_{2+i}^\star\cdot\boldsymbol{A}_3^\star + \frac{1}{2}\rho_\infty V_\infty^2 \boldsymbol{I}_D\cdot\boldsymbol{\mathcal{B}}_{2+i}\cdot\boldsymbol{A}_3 \end{aligned} \tag{16}$$

The aerodynamic loads (forces) of equation 15 are applied at the load points of the aerodynamic panels. They are transferred to the structural nodes using the algorithm applied for the steady case [8, 9].

The algorithm is the following. For all aerodynamic load points, the aerodynamic forces are extracted from equation 15. Then the triangular structural finite element that includes the load point of the generic aerodynamic panel is found. The equivalent loads applied at the nodes of the triangular FE element (which contains the load point) are obtained by using the area coordinates. Finally, an assembly procedure is required (a node in general connects more FE elements). Notice that some zero rows in correspondence of the rotational degrees of freedom have to be added.

From a practical point of view the matrices $\overline{\boldsymbol{\mathcal{A}}}_0$, $\overline{\boldsymbol{\mathcal{A}}}_1$, $\overline{\boldsymbol{\mathcal{A}}}_2$ and $\overline{\boldsymbol{\mathcal{A}}}_{2+i}$ are assembled at structural level [8]. $\boldsymbol{\mathcal{A}}_0^\star$ is the assembled matrix corresponding to $\overline{\boldsymbol{\mathcal{A}}}_0$. Similar notation is used for the other matrices. After the assembling is completed the vector of the aerodynamic forces applied at the nodes of the FE mesh is written as

$$\boldsymbol{L}_{\text{unsteady}}(s) = \left[\boldsymbol{\mathcal{A}}_0^\star + s\boldsymbol{\mathcal{A}}_1^\star + s^2\boldsymbol{\mathcal{A}}_2^\star + \sum_{i=1}^{\mathrm{N_{lag}}} \frac{s}{s+\beta_i}\boldsymbol{\mathcal{A}}_{2+i}^\star\right]\cdot\boldsymbol{U}(s) \tag{17}$$

The matrices $\boldsymbol{\mathcal{A}}_0^\star$, $\boldsymbol{\mathcal{A}}_1^\star$, $\boldsymbol{\mathcal{A}}_2^\star$ and $\boldsymbol{\mathcal{A}}_{2+i}^\star$ are obtained directly at full order structural level. "Full order" modeling leads, of course, to different size models for the structure and aerodynamics depending on the detail and number of degrees of freedom of structure and aerodynamics meshes, respectively. With full order aerodynamic models, on detailed aerodynamic meshes, it is possible to capture aerodynamic behavior due to local as well as global deformation patterns of the configuration.

4 TIME DOMAIN SIMULATIONS WITH AERODYNAMIC CONVOLUTION INTEGRALS (FIRST METHOD)

Starting point is equation 17. Using the Inverse Laplace Transform (ILT) expressions in the time domain can be obtained. To transform the lag terms to the time domain convolution integrals are used. The following definition is introduced:

$$\boldsymbol{\mathcal{A}}^\star \doteq \boldsymbol{\mathcal{A}}_0^\star + \sum_{i=1}^{\mathrm{N_{lag}}} \boldsymbol{\mathcal{A}}_{2+i}^\star \tag{18}$$

The time domain aerodynamic forces have can be demonstrated [8] to have the following form:

$${}^t\boldsymbol{L}_{\mathrm{unsteady}} = \boldsymbol{\mathcal{A}}^\star \cdot {}^t\boldsymbol{U} + \boldsymbol{\mathcal{A}}_1^\star \cdot {}^t\dot{\boldsymbol{U}} + \boldsymbol{\mathcal{A}}_2^\star \cdot {}^t\ddot{\boldsymbol{U}} - \sum_{i=1}^{\mathrm{N_{lag}}} \overline{\beta}_i \boldsymbol{\mathcal{A}}_{2+i}^\star \int_0^t {}^\tau\boldsymbol{U} e^{-\overline{\beta}_i(t-\tau)}\,\mathrm{d}\tau \tag{19}$$

The equation of motion, which includes aerodynamic and non-aerodynamic loads, has to be numerically integrated in the time. Newmark's method is used. The equation that has to be solved at each iteration of the Newton Raphson method is the following:

$$\boldsymbol{M}\cdot {}^{t+\Delta t}\ddot{\boldsymbol{U}}^n + \boldsymbol{C}_D \cdot {}^{t+\Delta t}\dot{\boldsymbol{U}}^n + {}^{t+\Delta t}\boldsymbol{K}_T^n \cdot {}^{t+\Delta t}\boldsymbol{u}^n = {}^{t+\Delta t}\boldsymbol{P}_{\mathrm{ext}} + {}^{t+\Delta t}\boldsymbol{L}_{\mathrm{unsteady}}^n - {}^{t+\Delta t}\boldsymbol{F}_{\mathrm{int}}^{(n-1)} \tag{20}$$

where ${}^{t+\Delta t}\boldsymbol{L}_{\mathrm{unsteady}}^n$ is the n^{th} realization of the aerodynamic loads at time $t+\Delta t$ and ${}^{t+\Delta t}\boldsymbol{P}_{\mathrm{ext}}$ are the external non-aerodynamic loads. The explicit form of the aerodynamic force vector is (see equation 19):

$${}^{t+\Delta t}\boldsymbol{L}_{\mathrm{unsteady}}^n = \boldsymbol{\mathcal{A}}^\star \cdot {}^{t+\Delta t}\boldsymbol{U}^n + \boldsymbol{\mathcal{A}}_1^\star \cdot {}^{t+\Delta t}\dot{\boldsymbol{U}}^n + \boldsymbol{\mathcal{A}}_2^\star \cdot {}^{t+\Delta t}\ddot{\boldsymbol{U}}^n - \sum_{i=1}^{\mathrm{N_{lag}}} \overline{\beta}_i \boldsymbol{\mathcal{A}}_{2+i}^\star \int_0^{t+\Delta t} {}^\tau\boldsymbol{U}^n e^{-\overline{\beta}_i(t+\Delta t-\tau)}\,\mathrm{d}\tau \tag{21}$$

The main problem is the calculation of the integrals in the time domain [8]. The details are omitted here for brevity. Note that the approximation used to calculate the integrals is more accurate if the size of the step used in the time integration is small. In order to have an indication of an opportune size of the time step the following formula was suggested:

$$\Delta t = \frac{2\pi b}{k_{\mathrm{max}}^\star V_\infty N_{\mathrm{time\ step}}} \tag{22}$$

$k_{\mathrm{max}}^\star = \frac{\omega_{\mathrm{max}} b}{V_\infty}$ is the maximum reduced frequency used for the Roger fit; $N_{\mathrm{time\ step}}$ is a number chosen by user. If this number is larger the accuracy is improved. CPU time increases considerably, however, when $N_{\mathrm{time\ step}}$ is large. Integrating in time using the present implicit method (Newmark's method) has the advantage that the high-frequency behavior, that is physically meaningless, is filtered out.
$\boldsymbol{C}_D$ is the full order damping matrix. A model for this matrix is presented in the authors' previous work [8]. Alternative models for the damping matrix can be assumed.

5 TIME DOMAIN SIMULATIONS USING SECOND ORDER UNSTEADY AERODYNAMIC EQUATIONS (SECOND METHOD)

This is an alternative procedure. It is extensively analyzed and compared with the first method [8] in reference [9]. The peculiarity of this procedure is that it avoids the needs of time domain integrals of the type seen for example in equation 19. As for the first method for time domain simulations the starting point is equation 17. Next, it is assumed that $\mathrm{N_{lag}}$, the number of lag terms, *is even*. Under this assumption the aerodynamic forces in the Laplace domain can be rearranged as follows:

$$\boldsymbol{L}_{\text{unsteady}}(s) = \left[\boldsymbol{\mathcal{A}}_0^\star + s\boldsymbol{\mathcal{A}}_1^\star + s^2\boldsymbol{\mathcal{A}}_2^\star\right]\boldsymbol{U}(s) + \left[\sum_{i=1}^{\mathrm{N_{lag}}/2} \frac{s\left(s+\overline{\beta}_{2i}\right)\boldsymbol{\mathcal{A}}_{1+2i}^\star + s\left(s+\overline{\beta}_{2i-1}\right)\boldsymbol{\mathcal{A}}_{2+2i}^\star}{\left(s+\overline{\beta}_{2i-1}\right)\left(s+\overline{\beta}_{2i}\right)}\right]\boldsymbol{U}(s) \tag{23}$$

Now the following definition is introduced:

$$\frac{s\left(s+\overline{\beta}_{2i}\right)\boldsymbol{\mathcal{A}}_{1+2i}^\star + s\left(s+\overline{\beta}_{2i-1}\right)\boldsymbol{\mathcal{A}}_{2+2i}^\star}{\left(s+\overline{\beta}_{2i-1}\right)\left(s+\overline{\beta}_{2i}\right)} \cdot \boldsymbol{U}(s) = \boldsymbol{\mu}_i(s) \tag{24}$$

$\boldsymbol{\mu}_i(s)$ is named *lag state variable*. There are $\mathrm{N_{lag}}/2$ lag state variables. The aerodynamic forces (equation 23) are then rewritten as

$$\boldsymbol{L}_{\text{unsteady}}(s) = \left[\boldsymbol{\mathcal{A}}_0^\star + s\boldsymbol{\mathcal{A}}_1^\star + s^2\boldsymbol{\mathcal{A}}_2^\star\right]\boldsymbol{U}(s) + \sum_{i=1}^{\mathrm{N_{lag}}/2}\boldsymbol{\mu}_i(s) \tag{25}$$

The lag state variables have to satisfy equation 24 which can be rearranged in a more convenient form:

$$s^2\boldsymbol{\mu}_i - s^2\boldsymbol{\mathcal{C}}_i\cdot\boldsymbol{U} + sB_i\boldsymbol{\mu}_i - s\boldsymbol{\mathcal{C}}_i^\star\cdot\boldsymbol{U} + B_i^\star\boldsymbol{\mu}_i = \boldsymbol{0} \tag{26}$$

where

$$\begin{aligned} B_i &= \overline{\beta}_{2i-1} + \overline{\beta}_{2i} \qquad B_i^\star = \overline{\beta}_{2i-1}\overline{\beta}_{2i} \\ \boldsymbol{\mathcal{C}}_i &= \boldsymbol{\mathcal{A}}_{1+2i}^\star + \boldsymbol{\mathcal{A}}_{2+2i}^\star \qquad \boldsymbol{\mathcal{C}}_i^\star = \overline{\beta}_{2i}\boldsymbol{\mathcal{A}}_{1+2i}^\star + \overline{\beta}_{2i-1}\boldsymbol{\mathcal{A}}_{2+2i}^\star \end{aligned} \tag{27}$$

Applying the Inverse Laplace Transform of both equations 26 and 25:

$$\begin{cases} {}^t\boldsymbol{L}_{\text{unsteady}} = \boldsymbol{\mathcal{A}}_2^\star\cdot{}^t\ddot{\boldsymbol{U}} + \boldsymbol{\mathcal{A}}_1^\star\cdot{}^t\dot{\boldsymbol{U}} + \boldsymbol{\mathcal{A}}_0^\star\cdot{}^t\boldsymbol{U} + \displaystyle\sum_{i=1}^{\mathrm{N_{lag}}/2}{}^t\boldsymbol{\mu}_i \\ {}^t\ddot{\boldsymbol{\mu}}_i - \boldsymbol{\mathcal{C}}_i\cdot{}^t\ddot{\boldsymbol{U}} + B_i{}^t\dot{\boldsymbol{\mu}}_i - \boldsymbol{\mathcal{C}}_i^\star\cdot{}^t\dot{\boldsymbol{U}} + B_i^\star{}^t\boldsymbol{\mu}_i = \boldsymbol{0} \end{cases} \tag{28}$$

The equation of motion, which includes aerodynamic and non-aerodynamic loads, has to be numerically integrated in the time. Newmark's method is used. The details are here omitted for brevity. With this formulation the tangent matrix of the entire system is calculated by including the contribution from the structure, the contribution from the aerodynamics and the dynamic contribution. This is also true for the case of the first method. The difference is that the mathematical expressions are not the same. Also, in the first method there are some auxiliary variables used to calculate the integrals in the time domain, whereas in the second approach there are other variables related to the lag terms. It can also be shown that the second method requires more memory to store the extra variables and matrices needed to carry out the iterative procedure [9].

6 TWO OPTIONS FOR THE DYNAMIC AEROELASTIC ANALYSIS

Regardless of which unsteady aerodynamic time domain method is used, two options for performing the time domain simulations are used here. In the first one, named "complete dynamic aeroelastic simulation", integration of the time dependent equations of motion is performed from the start, after the system is perturbed using initial shape (corresponding, for example, to a constant angle of attack) or some other initial conditions.

In the second option, named "dynamic aeroelastic perturbation about a steady state solution" the procedure is quite different. For the speed V_∞, the nonlinear steady state (static) equations are solved (Newton Raphson method). The static equilibrium configuration is represented by the coordinate vector $\boldsymbol{x}^{\text{eql}}$. Dynamic analysis is then performed about this static configuration. The two approaches have been compared in a previous paper [10]. In this work only the complete dynamic aeroelastic simulation is considered.

7 CONSISTENT FLUTTER SPEED $V_F^{\text{CONSISTENT}}$

For the case in which both the structural and aerodynamic models are assumed to be linear, the flutter speed is V_F^{linear}. In the present capability the linear flutter speed is calculated by using a root locus procedure based on a linear time invariant (LTI) state space model. A set of structural modes is used to calculate the generalized matrices. The linear flutter speed V_F^{linear} is calculated considering a basis of shapes (the modes in this paper) calculated in the reference configuration. Thus, the modes are calculated by using the linear stiffness matrix of the unloaded structure at the reference configuration with no initial angle of attack.
Viscous damping (indicated with ζ_i) may be used. For the simulations performed in this work the viscous damping is assumed to be zero.
For the proposed procedure presented in this work linear unsteady aerodynamics and geometrically nonlinear structural models are coupled. The definition of flutter speed is revised to account for "stability in the small" loss of stability about static aeroelastic solutions, where the local stiffness matrix (linear, geometric, and aerodynamic combined) replaces the reference linear stiffness matrix, and a "consistent" flutter speed is introduced as follows. A flow speed V'_∞, is selected. Given an initial perturbation from the reference unstressed shape of the structure (for example the structure is displaced with an angle of attack; in this paper it is used the perturbation $\alpha = 1\ deg$) a full order nonlinear static aeroelastic analysis is performed. The resulting deformed configuration now corresponds to the nonlinear static equilibrium at the assumed flow speed V'_∞. At this point, the tangent structural stiffness matrix relative to this configuration is calculated and used to find tangent structural modes. With these tangent modes a *linear* flutter analysis is carried out. The mode shapes in this case are relative to the deformed configuration. The resulting flutter speed V'_F can be larger, equal, or smaller than V'_∞ if the effect of internal stresses tend to reduce effective stiffness of the structure in the last case. The procedure is repeated [8] by increasing the air speed, calculating static aeroelastic deformation and internal stresses, calculating new structural modes for the stressed configuration, and then the resulting flutter speed for the linearization about the static aeroelastic solution. If the "stability in the small" flutter speed V'_F with respect to a stressed configuration at some airspeed V'_∞ is found to be equal to that airspeed, then, a "consistent" flutter speed has been found: $V_F^{\text{consistent}}$.
Validation of this procedure was presented for the case of a delta wing for which numerical

and experimental results are available [8].

8 RESULTS: JOINED WING WITH JOINT LOCATED AT 100% OF THE WING SPAN (JOINED WING MODEL I)

This joined wing is an aluminum wind tunnel model with cantilevered roots (see Figure 1). A detailed study of this model was performed in a previous work [10].

8.1 Nonlinear (Linearized) Flutter

The geometrical structural nonlinearity plays an important role in this configuration because of the internal in-plane forces in the joint area and upper wing. Table 1 presents some interesting results. Table 1 presents linearized flutter speeds about positions of static equilibria. The consistent flutter speed is found to be $V_F^{\text{consistent}} = 43\ m/s$ considerably higher than the linear flutter speed, which is for the same case $V_F^{\text{linear}} = 28.61\ m/s$.

8.2 Effect of Aerodynamic Speed on the Frequencies

Tracking the changes of "tangent" natural frequencies as a function of flight speed (and, thus, loading) can be very helpful when insight into the resulting aeroelastic behavior is sought [14, 15]. The changes of the first 6 frequencies are shown in Figure 2.

8.3 Linear and Nonlinear Static Aeroelastic Simulations

Table 2 shows aeroelastic linear displacements of three distinct points (on the lower wing, joint and upper wing respectively) as calculated by using the present code and NASTRAN. Table 2 validates the present static aeroelastic predictions for the case of a linear structure. Exploratory static aeroelastic simulations that include geometrical structural nonlinearities for the joined-wing case were carried out using the new capability. Results are shown in Figure 3. The nonlinear divergence speed can be found by increasing the aerodynamic speed V_∞. When the aeroelastic tangent matrix becomes singular the divergence speed is considered reached. Details of this procedure can be found in a previous publication [8].

8.4 Nonlinear Dynamic Aeroelastic Simulation

In an exploratory manner the full order dynamic aeroelastic simulation (nonlinear full order structural part and linear full order aerodynamic part) were applied to the joined wing model I. Figure 4 shows the time history of three points (on the lower wing, joint and upper wing respectively). For a subcritical case ($V_\infty = 30\ m/s < V_F^{\text{consistent}}$) after transients decay, the system converges to the steady state solution presented in Figure 3. The dynamic simulation of nonlinear aeroelastic behavior presents a bigger challenge when speeds close to or beyond the nonlinear divergence speed are considered. In a structurally nonlinear static solution that leads to buckling (divergence), the solution process, unless tailored to the task, can encounter convergence problems. Systematic studies of joined wing configurations at different speeds relative to their static and dynamic instability boundaries are necessary in order to fully understand the nonlinear aeroelastic behavior of such configurations.

9 RESULTS: JOINED WING WITH JOINT LOCATED AT 70% OF THE WING SPAN (JOINED WING MODEL II)

The model is shown in Figure 5.

9.1 Nonlinear (Linearized) Flutter

Table 3 shows the nonlinear (linearized) flutter speed and frequency when the speed corresponding to the initial nonlinear static equilibrium is changed. It can be observed that when the freestream speed is larger than $V_\infty = 20\ m/s$ the nonlinear effects become very important and the actual value of the linearized flutter speed changes considerably. In particular, for the linear case the flutter speed is $V_F^{\text{linear}} = 43.63\ m/s$. If the freestream speed V_∞ is increased (see Table 3) the *linearized* flutter speed calculated at the nonlinear static equilibrium corresponding to V_∞ changes as well. The consistent flutter speed is $V_F^{\text{consistent}} \approx 70\ m/s$ much higher than the linear flutter speed. This is not a general rule: if the configuration parameters are changed a different behavior may be observed.
The strong nonlinear effects that appear when the freestream speeds are higher than $V_\infty = 20\ m/s$ are also confirmed in the Figures 6-9 discussed in the next section.
The joined wing model I presented similar property and the consistent flutter speed was much higher than the linear flutter speed (see Table 1).

9.2 Effect of Aerodynamic Speed on the Frequencies

The changes of the first 7 frequencies are shown in Figure 10. The complex nonlinear nature of this joined wing is particularly evident for high order frequencies.

9.3 Linear and Nonlinear Static Aeroelastic Simulations

Figures 6-9 show the linear and nonlinear aeroelastic deflections at several points located on the inboard wing, outboard wing, joint and upper wing (points P_1, P_2, P_3 and P_4 respectively). It is possible to see that in the nonlinear case the deflection of point P_4 is smaller than the corresponding displacement for the linear case. Also, the excellent correlation of the present capability (1088 aerodynamic panels are used) with NASTRAN (720 aerodynamic panels are used) can be observed.
In all the cases the curves representing the linear and nonlinear displacements are almost coincident for $V_\infty \leq 20 m/s$. For higher freestream velocities the structural nonlinear effects become very important and the displacement curves are significantly different. In that cases the structural nonlinearity must be taken into account for an accurate aeroelastic description of the joined wing model.

10 CONCLUSIONS

Previous publications discussed a nonlinear aeroelastic procedure for coupling linear modally reduced generalized unsteady aerodynamic forces (GAF, as commonly calculated by standard unsteady aerodynamics codes such as Doublet Lattice, PANAIR, ZAERO) with geometrically nonlinear full order structural finite element equations. The procedure can also use GAFs generated about a nonlinear CFD solution by linearized CFD solutions or by modal perturbations of CFD solutions with respect to their steady state reference. That

procedure was also extended to couple nonlinear structural finite element codes with full order linear unsteady aerodynamic models on their full order aerodynamic meshes.

Treatment in the time domain of unsteady aerodynamics can be done in two ways: use convolution integrals based on first order ODE models of the lag terms, or use second order ODE models for the aerodynamic lag terms without any convolution integrals.

The solution can be carried out either as a complete dynamic simulation starting with the unstressed reference structure and some initial conditions in the form of an initial perturbation shape, or, alternatively, start with a static aeroelastic solution at the speed of interest, and follow up by a dynamic perturbation simulation about the resulting nonlinear aeroelastic steady state.

Exploratory studies (linear and nonlinear) of 2 prototype experimental joined wing configurations have been carried out and reported, together with a discussion of the possible aeroelastic complexity of these configurations. The effect of the spanwise position of the joint has been analyzed and discussed. It has been shown that the effects of the geometrically nonlinear structures can change the static and dynamic aeroelastic properties of the wings significantly. The joint location affects the nonlinear linearized flutter speed. In this work 2 joint positions have been analyzed. The first one is at 100% of the wing span (joined wing model I). The second one is at 70% of the wing span (joined wing model II). The joined wing model II presents a nonlinear linearized flutter speed 50% higher than the flutter speed found for the joined wing model I. In both cases the consistent flutter speed, the speed at which the linearized system about a steady equilibrium loses stability at that point, is higher than the linear flutter speed. This example shows the importance of an accurate description of the geometrically nonlinear structural effects for the correct representation of the joined wings' behavior.
Other parameters should be changed to study the sensitivity of the aeroelastic response. In particular, the effects of the outer wing in the case of joined wing model II are of particular interest as far as the consistent flutter speed is concerned.

11 REFERENCES

[1] Livne, E. (2001). Aeroelasticity of joined-wing airplane configurations - past work and future challenges - a survey. AIAA Paper 2001-1370, AIAA. Presented at the 42nd AIAA/ASME/ASCE/AHS/ASC Structures, Structural Dynamics, and Materials Conference, Seattle, WA, Apr. 16-19.

[2] Geuzaine, P., Brown, G., Harris, C., et al. (2003). Aeroelastic dynamic analysis of a full f-16 configuration for various flight conditions. *AIAA Journal*, 41(3), 363–371.

[3] Maute, K., Nikbay, M., and Farhat, C. (2001). Coupled analytical sensitivity analysis and optimization of three-dimensional nonlinear aeroelastic systems. *AIAA Journal*, 39(11), 2051–2061.

[4] Magnus, A. E. and Epton, M. A. (1980). Pan air-a computer program for predicting subsonic or supersonic linear potential flows about arbitrary configurations using a higher order panel method. Tech. rep. Vol. 1. Theory Document (Version 1.0), NASA CR-3251.

[5] Chen, P. and Liu, D. (1990). Unsteady supersonic computations of arbitrary wing-body configurations including external stores. *Journal of Aircraft*, 27(2), 108–116.

[6] Chen, P., Lee, H., and Liu, D. (1993). Unsteady subsonic aerodynamics for bodies and wings with external stores including wake effect. *Journal of Aircraft*, 30(5).

[7] ZONA Thechnology, I. (2004). Zaero. Tech. rep. Theoretical Manual, Version 7.1.

[8] Demasi, L. and Livne, E. (2009). Dynamic aeroelasticity of nonlinear configurations using linear modally reduced aerodynamic generalized forces. *AIAA Journal*, 47(1), 71–89.

[9] Demasi, L. and Livne, E. (2009). Aeroelastic coupling of geometrically nonlinear structures and linear unsteady aerodynamics: Two formulations. *Journal of Fluids and Structures, in press.*

[10] Demasi, L. and Livne, E. (2008). Dynamic aeroelasticity coupling full order geometrically nonlinear structures and full order linear unsteady aerodynamics - the joined wing case. AIAA Paper 2008-1818, AIAA. Presented at the 49th AIAA/ASME/ASCE/AHS/ASC Structures, Structural Dynamics, and Materials Conference, Schaumburg, IL, Apr. 7-10.

[11] Levy, R. and Gal, E. (2003). Triangular shell element for large rotations analysis. *AIAA Journal*, 41, 2505–2508.

[12] Levy, R. and Spillers, W. (2003). *Analysis of Geometrically Nonlinear Structures.* 2nd edition, Kluwer Academic Publishers, Dordrecht, Boston, ISBN 1402016549.

[13] Gal, E. and Levy, R. (2005). The geometric stiffness of triangular composite-materials shell elements. *Computers and Structures*, 83, 2318–2333.

[14] Patil, M. J. (2003). Nonlinear aeroelastic analysis of joined-wing aircraft. Tech. rep., AIAA. Presented at the 44th AIAA/ASME/ASCE/AHS/ASC Structures, Structural Dynamics, and Materials Conference, Norfolk, Virginia, Apr. 7-10.

[15] Oliver, M., Climent, H., and Rosich, F. (1999). Nonlinear effects of applied loads and large deflections on aircraft normal modes. Tech. rep. RTO (NATO) Meeting Proceedings 36 on Structural Aspects of Flexible Aircraft Control.

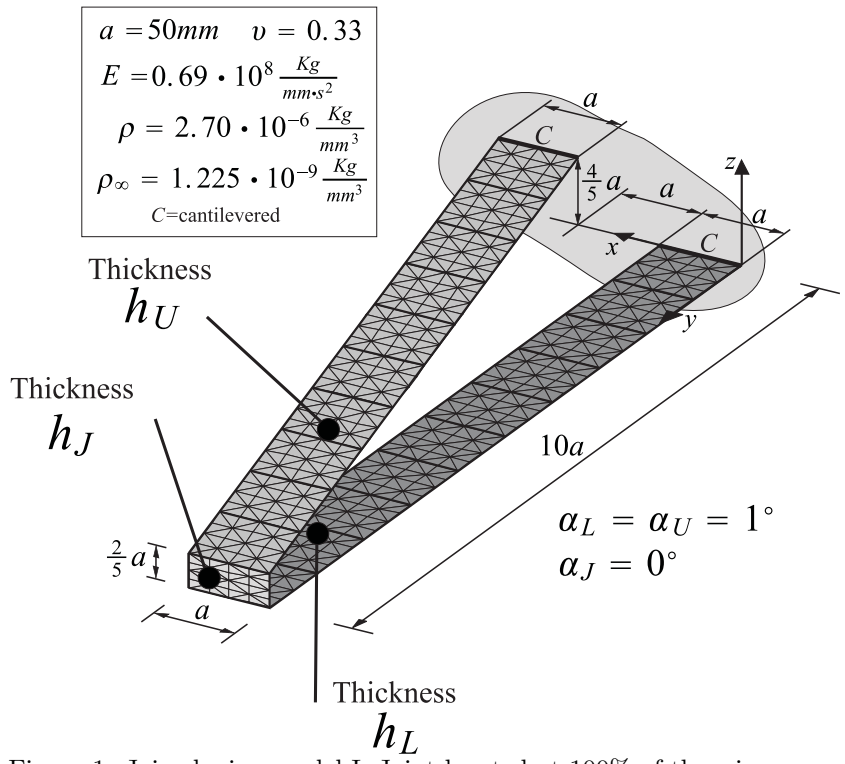

Figure 1: Joined wing model I. Joint located at 100% of the wing span.

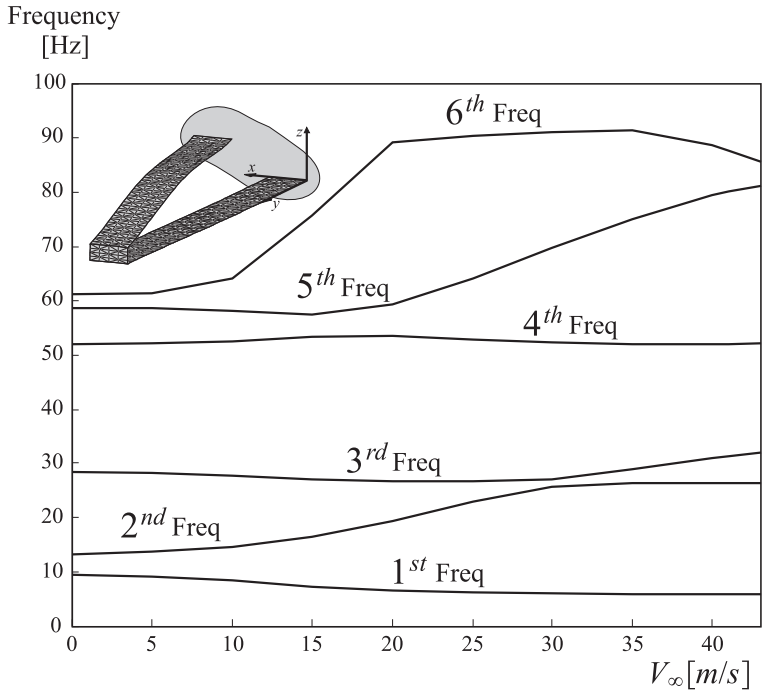

Figure 2: Joined wing model I. Structural "tangent" frequencies $[Hz]$ (present capability with 952 aerodynamic panels used for the aerodynamic model). Lower wing, joint and upper wing have thickness $h_L = 2.0\ mm$, $h_J = 2.0\ mm$ and $h_U = 0.5\ mm$ respectively. The free vibration problem is solved at the equilibrium steady state corresponding to V_∞ (the structural tangent matrix at that point is considered).

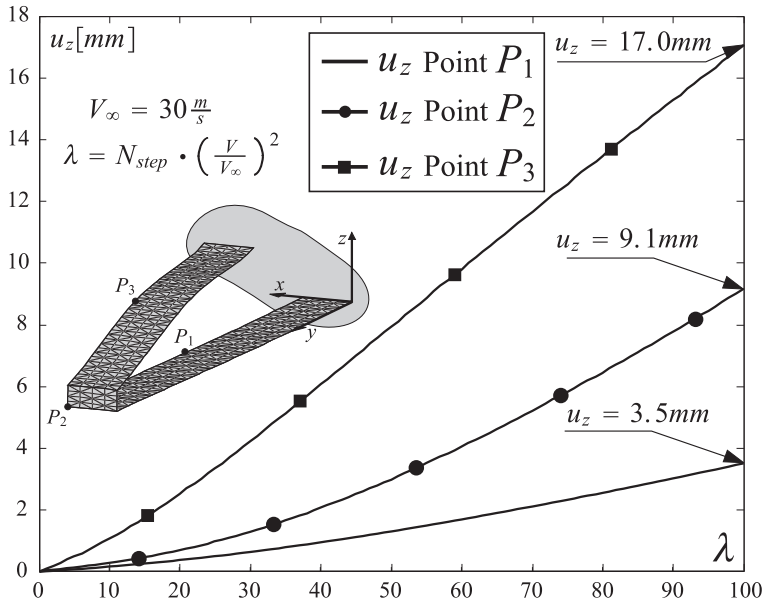

Figure 3: Joined wing model I. Nonlinear steady state solution (present capability, $V_\infty = 30\ m/s$, present capability, 952 aerodynamic panels). Lower wing, joint and upper wing have thickness $h_L = 2.0\ mm$, $h_J = 2.0\ mm$ and $h_U = 0.5\ mm$ respectively. $P_1 \equiv (a, 5a, 0)$; $P_2 \equiv (a, 10a, 0)$; $P_3 \equiv (2a, 5a, \frac{3}{5}a)$; $a = 50\ mm$.

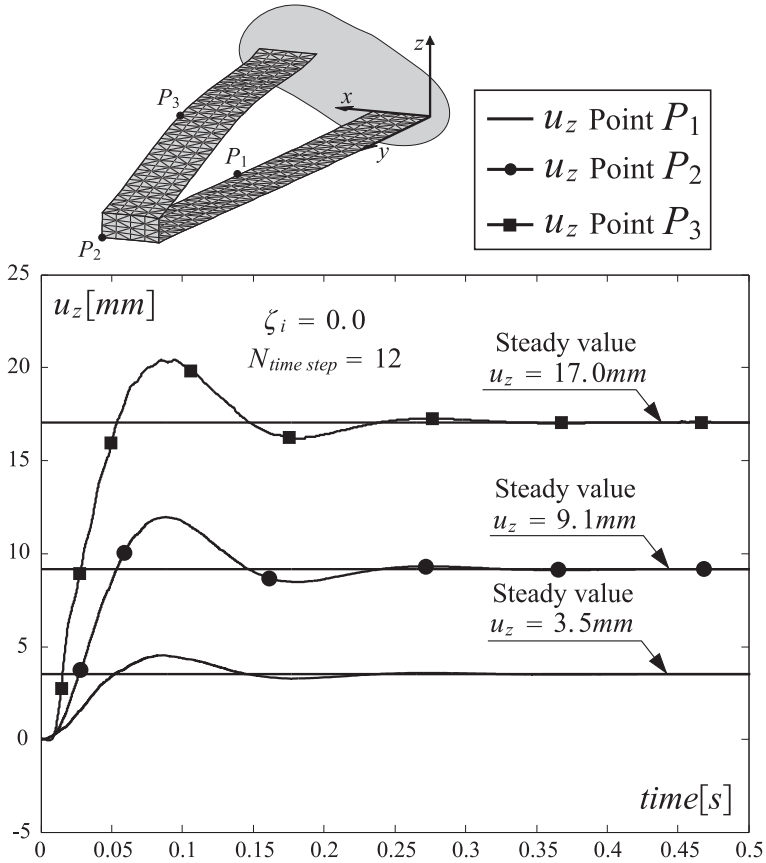

Figure 4: Joined wing model I. Nonlinear time-domain simulation (sub-critical case, $V_\infty = 30\ m/s$, present capability, 952 aerodynamic panels). In all cases $\zeta_i = 0$. Lower wing, joint and upper wing have thickness $h_L = 2.0\ mm$, $h_J = 2.0\ mm$ and $h_U = 0.5\ mm$ respectively. $P_1 \equiv (a, 5a, 0)$; $P_2 \equiv (a, 10a, 0)$; $P_3 \equiv (2a, 5a, \frac{3}{5}a)$; $a = 50\ mm$. Time domain simulation conducted by using convolution integrals for the aerodynamic lag terms.

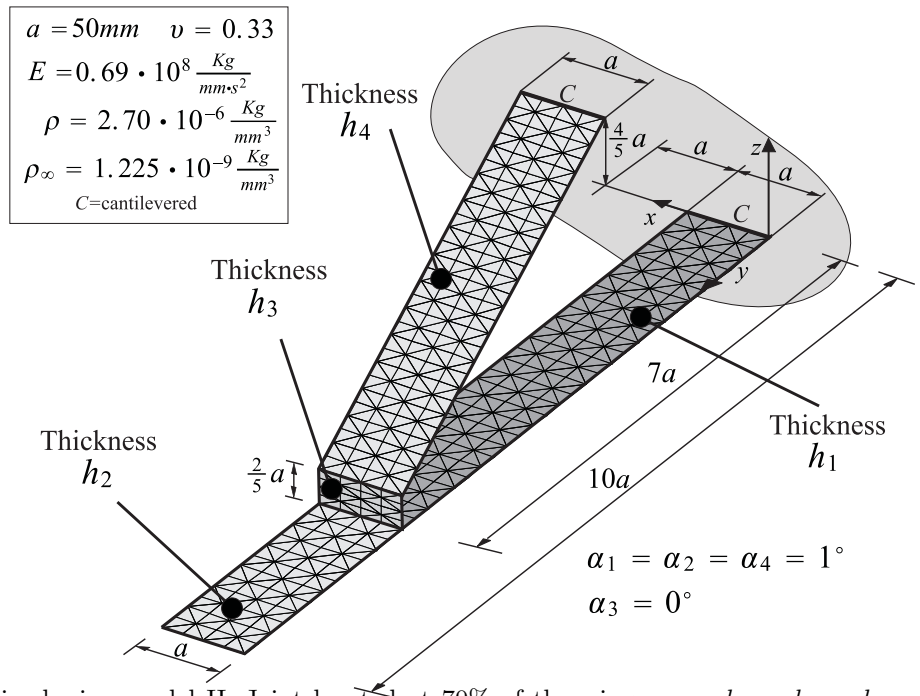

Figure 5: Joined wing model II. Joint located at 70% of the wing span. $h_1 = h_2 = h_3 = 2mm$; $h_4 = 0.5mm$

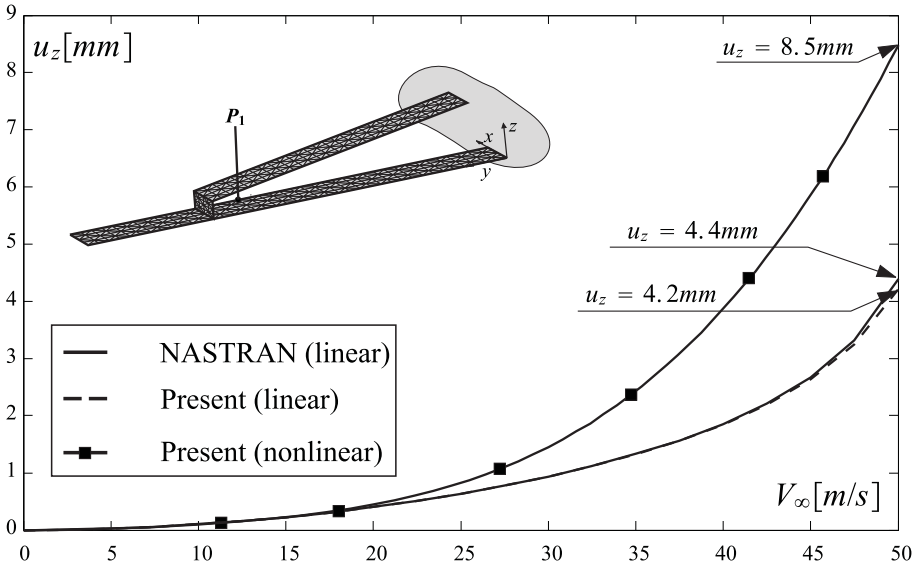

Figure 6: Joined wing model II. Linear and nonlinear steady deflection u_z at point $P_1 \equiv (a, 6a, 0)$; $a = 50\ mm$. Comparison (for the linear case only) against NASTRAN (SOL 144).

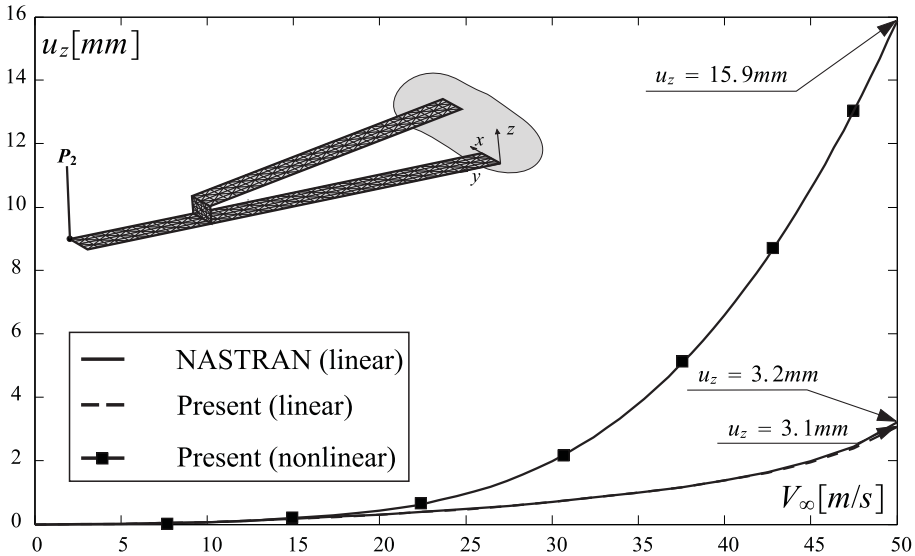

Figure 7: Joined wing model II. Linear and nonlinear steady deflection u_z at point $P_2 \equiv (a, 10 \cdot a, 0)$; $a = 50\ mm$. Comparison (for the linear case only) against NASTRAN (SOL 144).

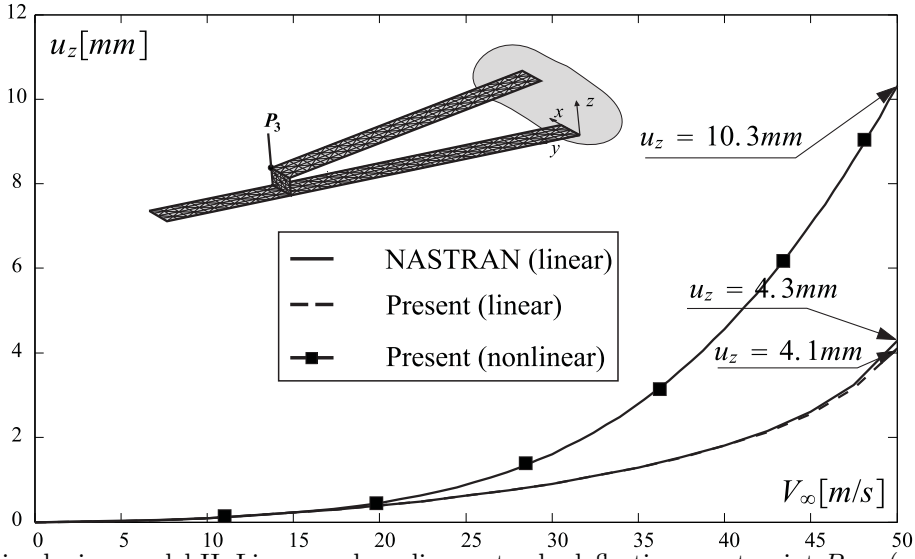

Figure 8: Joined wing model II. Linear and nonlinear steady deflection u_z at point $P_3 \equiv (a, 7 \cdot a, 2/5 \cdot a)$; $a = 50\ mm$. Comparison (for the linear case only) against NASTRAN (SOL 144).

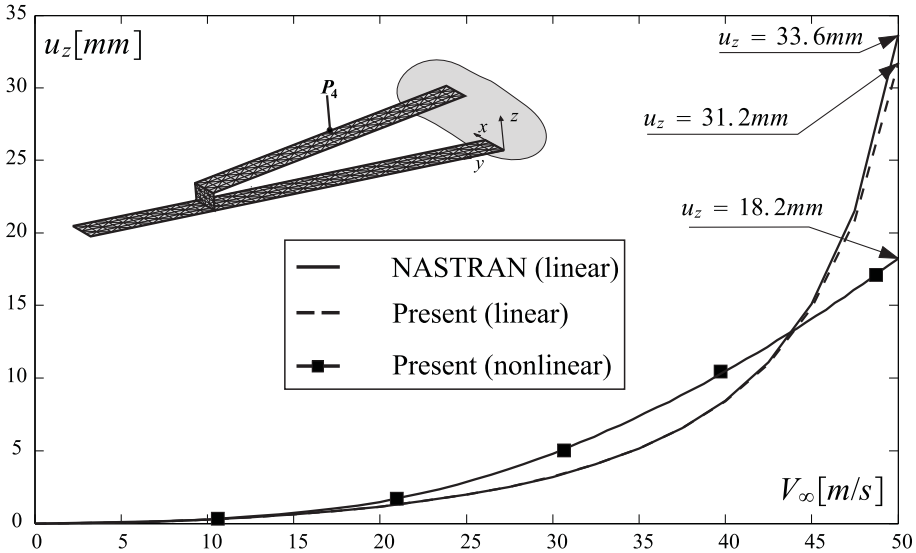

Figure 9: Joined wing model II. Linear and nonlinear steady deflection u_z at point $P_4 \equiv (29/14 \cdot a, 13/4 \cdot a, 43/70 \cdot a)$; $a = 50\ mm$. Comparison (for the linear case only) against NASTRAN (SOL 144).

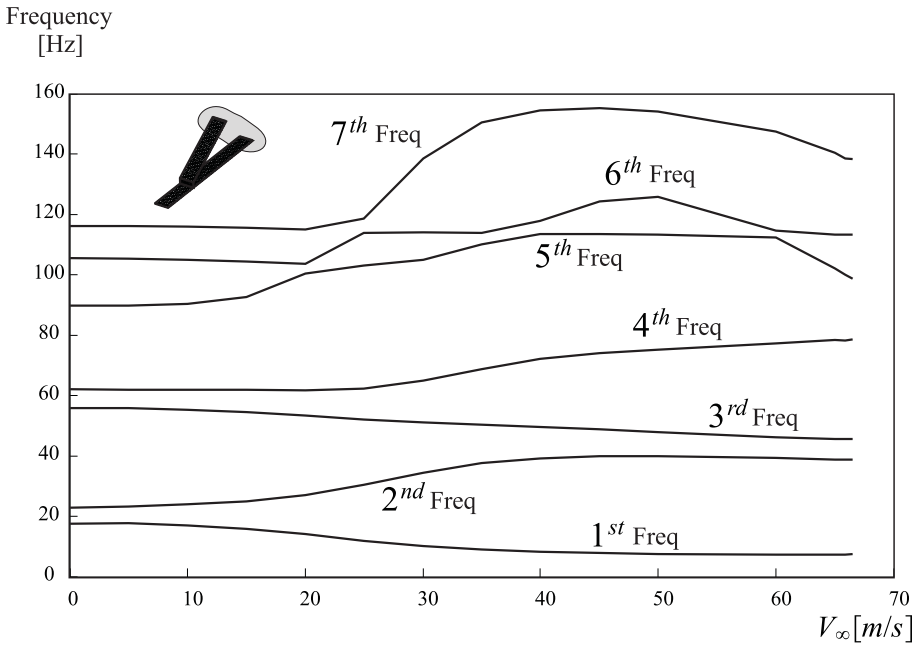

Figure 10: Joined wing model II. Structural "tangent" frequencies $[Hz]$ (present capability with 1088 aerodynamic panels used for the aerodynamic model). The free vibration problem is solved at the equilibrium steady state corresponding to V_∞ (the structural tangent matrix at that point is considered).

Table 1: Joined wing model I. Nonlinear (linearized) flutter speed V_F and frequency f_F for the Joined Wing model (present capability with 952 aerodynamic panels used for the aerodynamic model). In all cases $\zeta_i = 0$. Lower wing, joint and upper wing have thickness $h_L = 2.0mm$, $h_J = 2.0mm$ and $h_U = 0.5mm$ respectively. In all cases 40 modes have been used for the calculation of the generalized matrices. The flutter speed is calculated after a linearization at the equilibrium steady state corresponding to V_∞. When $V_\infty = V_F$ the "consistent" flutter speed is reached.

V_∞	V_F $[m/s]$	f_F $[Hz]$
0	28.61	39.81
5	28.75	40.02
10	30.03	41.62
15	29.11	59.09
20	39.35	66.86
25	44.39	73.37
30	45.68	75.61
35	44.77	76.19
40	43.96	74.28
41	43.63	73.71
43	42.71	72.59

Table 2: Joined wing model I. Linear steady deflection u_z at points P_1, P_2 and P_3. Comparison against NASTRAN (SOL 144). $h_L = 2.0\ mm$, $h_J = 2.0\ mm$, $h_U = 0.5\ mm$. $P_1 \equiv (a, 5a, 0)$; $P_2 \equiv (a, 10a, 0)$; $P_3 \equiv (2a, 5a, \frac{3}{5}a)$; $a = 50\ mm$.

$V_\infty[m/s]$	$u_z[mm]$ point P_1	$u_z[mm]$ point P_2	$u_z[mm]$ point P_3
NASTRAN, 840 aerodynamic panels			
5	$4.46 \cdot 10^{-2}$	$6.51 \cdot 10^{-2}$	$2.51 \cdot 10^{-1}$
10	$1.81 \cdot 10^{-1}$	$2.65 \cdot 10^{-1}$	1.06
15	$4.19 \cdot 10^{-1}$	$6.15 \cdot 10^{-1}$	2.66
20	$7.86 \cdot 10^{-1}$	1.16	5.62
25	1.35	2.01	11.56
26	1.51	2.24	13.47
27	1.68	2.51	15.81
Present capability, 952 aerodynamic panels			
5	$4.48 \cdot 10^{-2}$	$6.55 \cdot 10^{-2}$	$2.55 \cdot 10^{-1}$
10	$1.82 \cdot 10^{-1}$	$2.66 \cdot 10^{-1}$	1.08
15	$4.22 \cdot 10^{-1}$	$6.18 \cdot 10^{-1}$	2.70
20	$7.89 \cdot 10^{-1}$	1.16	5.70
25	1.36	2.01	11.68
26	1.51	2.24	13.59
27	1.68	2.51	15.91

Table 3: Joined wing model II. Nonlinear (linearized) flutter speed V_F and frequency f_F for the Joined Wing model (present capability, 1088 aerodynamic panels). In all cases $\zeta_i = 0$. In all cases 40 modes have been used for the calculation of the generalized matrices. The flutter speed is calculated after a linearization at the equilibrium steady state corresponding to V_∞. For the linear case the flutter speed and frequency calculated with NASTRAN are $V_F = 42.65$ $[m/s]$ and $f_F = 52.43$ $[Hz]$ respectively. When $V_\infty = V_F$ the "consistent" flutter speed is reached.

V_∞	V_F $[m/s]$	f_F $[Hz]$
0.00	43.63	51.60
5.00	43.82	51.66
10.0	44.54	51.74
15.0	43.14	62.41
20.0	44.99	68.38
25.0	51.10	80.08
30.0	60.21	91.46
35.0	63.91	116.20
40.0	68.00	117.97
45.0	69.19	120.35
50.0	73.24	116.74
60.0	70.52	116.82
65.0	67.38	114.45
65.9	67.39	113.32
66.5	66.93	113.48
68.0	62.46	114.14
70.0	63.03	109.77